Science of the Total Environment 915 (2024) 170008

Contents lists available at ScienceDirect

Science of the Total Environment

journal homepage: www.elsevier.com/locate/scitotenv

Automated SEM/EDX imaging for the in-depth characterization of non-exhaust traffic emissions from the Munich subway system

Carsten Neukirchen [a,d], Thorsten Meiners [b], Jan Bendl [a,e,*], Ralf Zimmermann [c,d], Thomas Adam [a,c]

[a] University of the Bundeswehr Munich, Faculty for Mechanical Engineering, Institute of Chemical and Environmental Engineering, Werner-Heisenberg-Weg 39, 85577 Neubiberg, Germany
[b] Oxford Instruments GmbH, Borsigstraße 15 A, 652025 Wiesbaden, Germany
[c] Joint Mass Spectrometry Center (JMSC) at Comprehensive Molecular Analytics (CMA), Department Environmental Health, Helmholtz Munich, Gmunder Str. 37, 81379 München, Germany
[d] Joint Mass Spectrometry Center (JMSC) at Chair of Analytical Chemistry, Institute of Chemistry, University of Rostock, Albert-Einstein-Strasse 27, 18059 Rostock, Germany
[e] Institute for Environmental Studies, Faculty of Science, Charles University, Benátská 2, 128 01 Prague, Czech Republic

HIGHLIGHTS

- Majority of particles formed from abrasion of brakes, rails and wheels.
- 94–97 % of ≥1 μm and 63 % of particles ≤1 μm classified as highly ferruginous.
- Heavy metal particles found also in the ultrafine size range.
- Particle number mode detected between 200 and 300 nm.
- The utilized method classifies up to 99 % of over 200,000 particles.

GRAPHICAL ABSTRACT

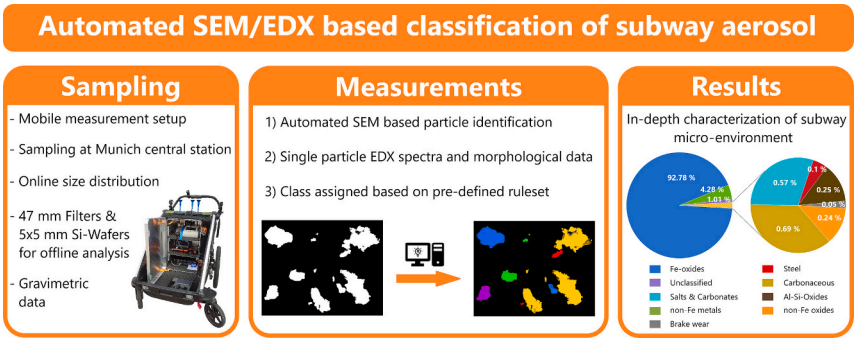

ARTICLE INFO

Editor: Hai Guo

Keywords:
Automated particle classification
Train emissions
Personal exposure

ABSTRACT

A SEM/EDX based automated measurement and classification algorithm was tested as a method for the in-depth analysis of micro-environments in the Munich subway using a custom build mobile measurements system. Sampling was conducted at platform stations, to investigate the personal exposure of commuters to subway particulate matter during platform stays. EDX spectra and morphological features of all analyzed particles were automatically obtained and particles were automatically classified based on pre-defined chemical and morphological boundaries. Source apportionment for individual particles, such as abrasion processes at the

Abbreviations: AR, Aspect ratio; BSE, Backscattered electrons; EAD, Equivalent aerodynamical diameter; ECD, Equivalent circular diameter; EPD, Equivalent perimeter diameter; EDX, Energy-dispersive X-ray spectroscopy; EHT, Electron high tension; FePM, Iron rich particulate matter; ICP-MS, Inductively coupled plasma mass spectrometry; NEE, Non-exhaust emissions; NP, Nanoparticle; OPS, Optical particle sizer; PC, Polycarbonate; PM, Particulate matter; PNC, Particle number concentration; ROS, Reactive oxygen species; SEM, Scanning electron microscopy; SI, Supplementary information.

* Corresponding author at: University of the Bundeswehr Munich, Faculty for Mechanical Engineering, Institute of Chemical and Environmental Engineering, Werner-Heisenberg-Weg 39, 85577 Neubiberg, Germany.
E-mail address: jan.bendl@unibw.de (J. Bendl).

https://doi.org/10.1016/j.scitotenv.2024.170008
Received 19 November 2023; Received in revised form 27 December 2023; Accepted 6 January 2024
Available online 12 January 2024

Elemental composition
Algorithm-based particle classification
Scanning electron microscopy

wheel-brake interface, was partially possible based on the established particle classes. An average of 98.87 ± 1.06 % of over 200,000 analyzed particles were automatically assigned to the pre-defined classes, with 84.68 ± 16.45 % of particles classified as highly ferruginous. Manual EDX analysis further revealed, that heavy metal rich particles were also present in the ultrafine size range well below 100 nm.

1. Introduction

Exhaust particle emissions have long been known to be harmful and to cause diseases, such as inflammatory lung diseases and lung cancer (Ghio et al., 2012; Totlandsdal et al., 2010). With modern day regulations becoming stricter, exhaust emissions have declined throughout the last decades reaching a point where automotive non-exhaust emissions (NEE), such as brake and tyre abrasion, have surpassed engine exhaust emissions as largest traffic derived contributors to urban PM_{10} pollution (Grigoratos and Martini, 2014). Some NEE's like automotive brake and tyre particles, which will be included for the first time in the upcoming EURO 7 norm, are currently undergoing legislatory processes (Storch et al., 2023), however, most of them are still unregulated. Nonetheless NEE's are of rapidly growing interest for researchers worldwide, which is due to their potential as environmental pollutants and hazardous substances. NEE's are mainly abrasion derived particles, formed from braking processes or friction between wheels and roads/rails. While tyre abrasion particles contribute greatly to the microplastic problem (Knight et al., 2020), other NEE's released from brake pads and train steel wheels and rails consist mainly of heavy metals (Font et al., 2019; Grigoratos and Martini, 2015). Particles bearing high quantities of heavy metals are known to induce chronic respiratory diseases and to facilitate lung cancer via the formation of reactive oxygen species (ROS) through the Fenton reaction causing DNA damage in the respiratory tract (Kanti Das et al., 2014). Small particles are of special concern with $PM_{2.5}$ being able to penetrate deep into the lungs and particles smaller than 0.1 μm depositing in the alveoli, eventually reaching the bloodstream via the blood-air barrier (Bachler et al., 2015). Furthermore metal containing nanoparticles (NP) were found to penetrate to the central nervous system via uptake and transport in the olfactory nerve via the nasal route (Hopkins et al., 2018; T. Fortoul et al., 2015) causing pro-inflammatory responses (Trickler et al., 2014) as well as apoptosis due to increased cytotoxicity of heavy metals (Niska et al., 2015).

While most techniques for elemental analysis, such as conventional ICP-MS, are capable of measuring trace quantities of elements in whole samples, they cannot distinguish, whether a certain element is distributed homogenously among all particles or if high quantities are present in a small number of particles. While recently more specialized techniques, such as single particle ICP-MS with time-of-flight based detection for chemical characterization of particles arise, they are still limited regarding their measurable size range (Laborda et al., 2014) and are generally more applicable to the analysis of aqueous and powder samples, instead of aerosols, which are normally sampled on filters. In contrast, EDX analysis provides spectra for thousands of individual particles regardless of their source, thus offering the possibility of addressing the homogeneity of complex environmental samples. This benefit is of special interest for the characterization of subway aerosols, where highly redox active, copper-rich particles derived from sparking at the catenary-pantograph-interface (Font et al., 2019) as well as abrasion derived metallic and oxidic iron particles frequently occur (Bendl et al., 2023; Font et al., 2019). Especially copper NP quantities are critical in closed, poorly ventilated environments like subways, given that they are considered to be among the most toxic particles in mammals (Hejazy et al., 2018). In addition to their size and the chemical composition, form factors play an important role in particle toxicity. While the health impact of inhalable iron oxide particles is commonly regarded as low, subway emissions have been shown to be of increased cytotoxicity (Jung et al., 2012; Loxham and Nieuwenhuijsen, 2019) linked to the large surface area of abrasion derived particles, which often exhibit rough and splintery edges (Moreno et al., 2015).

Automated Imaging software offers a powerful solution for the characterization of large amounts of individual features rendering them an ideal tool for morphology-based particle characterization with the SEM. If a particle is identified, its morphological data is automatically measured and a subsequent EDX measurement is triggered by the software supplying additional chemical data used for classification. A set of classification boundaries is then applied to the dataset sorting the analyzed features into pre-defined categories. Parameters utilized for classification can either be directly measured geometrical values, such as the length (also known as maximum feret diameter) and the perimeter of a particle, or calculated values like the equivalent circular diameter (ECD) and the aspect ratio as well as the elemental composition. This approach can be utilized to accomplish a variety of objectives, such as analyzing the homogeneity of particles, or solving so called "needle in a haystack" problems, where small quantities of particles of interest (e.g. copper particles from sparking at the catenary/ third-rail type power supply) are scattered among a large number of other particles. Furthermore, the Imaging Software ZEN core (Carl Zeiss) was used to obtain high-resolution morphological data for the bulk of the particles.

The aim of this study was to demonstrate a new approach in detailed elemental analysis of particles using automated SEM/EDX, which allows almost all particles captured on the filter to be analyzed separately for their elemental composition and morphology, and to be classified based on the data obtained. This approach could have wide applications in aerosol research and air quality measurement. We have demonstrated this method in the context of mobile air quality measurements in the Munich subway (Bendl et al., 2023), assessing the personal exposure of commuters to harmful compounds such as heavy metals at the subway platform. To the best of our knowledge, there is no published study on individual particle compositions in subway systems worldwide with a data-set of comparable size with over 200,000 particles automatically analyzed and classified yielding detailed results with a statistically relevant sample size.

2. Methods and materials

2.1. Sampling and studied location

All samples were collected in the Munich subway (Germany) in the middle of the platform of the central station, called "Hauptbahnhof" (line U4/U5), at exactly the same spot. As a housing for all the instruments, a self-made mobile measuring system consisting of an aluminum ventilated box with omni-directional inlets (801565, TSI), located in the breathing zone height of a seated person was used (Bendl et al., 2023). The platform is located below ground in a depth of - 22 m (DB Netz AG, 2023). A map of the Munich subway system with a photo of the sampling site highlighted in the map, as well as the mobile measurement device used in this study are shown in Fig. 1.

Sample 1 was collected on 17/5/2022 (14:08–17:08) using a pump with a constant flowrate of 8.5 lpm (SG10-2, GSA) and a $PM_{2.5}$ pre-impactor (Sioutas, SKC; $PM_{2.5}$ fraction). Sample 2 was collected using the same set-up on 19/7/2022 (20:33–23:21), but without the pre-impactor (PM_{total} fraction). Sample 3 was collected on 28/8/2023 (14:06–20:06) without any pre-impactor (PM_{total} fraction) over a longer period of time, therefore, a sampler with a lower flow rate of 2 lpm was used (BiVOC2V2, Holbach) to make sure that filters were not overloaded. The method can operate in a wide range of particle concentrations, as long as there are enough particles on a filter to be statistically

representative and individual particles are present, which do not overlap due to overloading.

Particles were sampled on 47 mm polycarbonate (PC) track-etched filters (Whatman, Nuclepore, 2 μm pore-size), with five silica wafers (p-type boron dotted 5 × 5 mm, Ted Pella Inc.) placed on-top of each filter, situated in vertically positioned filter-holders so that wafers were at fixed positions over the whole sampling time.

To prevent contaminations, sampling for gravimetric analysis was performed using an additional identical pump (SG10-2, GSA), 47 mm filter holder, and a PC filter, which was weighed prior and after sampling using a micro-balance (Cubis MCA2.7S-2S00-F, Sartorius) and pre-conditioned (45 % RH, 22 °C) for 24 h in a weighing chamber (pureGMC 18-EPA1065) with a corona discharger for filter charge neutralization (Bendl et al., 2023).

All flowrates of the pumps were set/checked using a mass flow meter (4043H, TSI).

2.2. Online particle measurements

During the sampling period, the PM size-distribution in the range of 0.3–10 μm was measured with a resolution of 1 Hz via an Optical Particle Sizer (OPS 3330, TSI). On-line data was corrected based on gravimetry with a factor of 2.11 (Bendl et al., 2023). Particle number concentrations (PNC) in the range of 10–700 nm were measured in 1 Hz using a DISCmini from Testo.

2.3. Sample preparation

Samples with a diameter of 12 mm were cut from each filter and were transferred to SEM pin stubs with conductive high purity EDX suitable double-sided carbon adhesive pads in-between (Spectro-Tabs, Plano GmbH company). Silica wafers were secured to SEM pin stubs with conductive silver paint (EM-Tec AG15, Micro to Nano). Wafers and filter punches were then stored in a desiccator under vacuum for 24 h to ensure removal of volatile components that would otherwise contaminate the system. The wafer surface was left unaltered, while filter samples were coated with a conductive carbon layer of approximately 10 nm, to minimize charging effects during analysis. Surface coating was applied with a Q150T ES Plus sputter device (Quorum technologies) utilizing a woven carbon fiber string (density 1.55 g/m, Quorum technologies) in pulsed cord evaporation mode.

2.4. SEM/EDX analysis

SEM micrographs were taken with the Inlens and SE2 detectors of a Gemini Sem 360 (Carl Zeiss) field emission SEM at acceleration voltages of 0.75–1.5 kV. Manual EDX analysis was conducted with an UltimMax 40 EDX detector (Oxford Instruments). Additionally, samples were measured via the manufacturers Software ZEN core EM 3.5 to obtain high resolution morphological data for the calculation of size and shape descriptors. Particles were imaged with a 5 nm pixel size with a minimum particle length of 100 nm and a minimum breath of 50 nm.

Automated SEM/EDX measurements were conducted with a Zeiss Gemini 450 SEM equipped with an UltimMax 170 EDX detector and an UltimExtreme windowless EDX detector from Oxford Instruments. The UltimMax 170 is an ultra large area Silicon Drift Detector (170 mm^2 detection area) equipped with a thin polymer window allowing high count rates and, therefore, short acquisition times. The UltimExtreme is a 100 mm^2 windowless detector with an optimized geometry and electron trap allowing to reach very small detector to sample distances and thus large solid angles. It is optimized for low kV analysis and reaches high count rates compared to conventional detectors, even with low beam currents. The Software AZtec Feature (Version 6.0) was used for automated detection of particles based on their mean gray value measured with a backscatter electron detector (BSE). The electron yield of a common BSE detector strongly depends on the mean atomic number of the analyzed material (Čalkovský et al., 2023). In this way, particles can be easily separated from the substrate (in this work carbon adhesive pads and Si wafer) by gray values of the BSE detector, if particles are heavier or lighter than the substrate. The automated particle analysis was carried out at 15 kV for all samples as well as at 5 kV for the carbon pad samples in order to reduce the interaction volume of the incoming

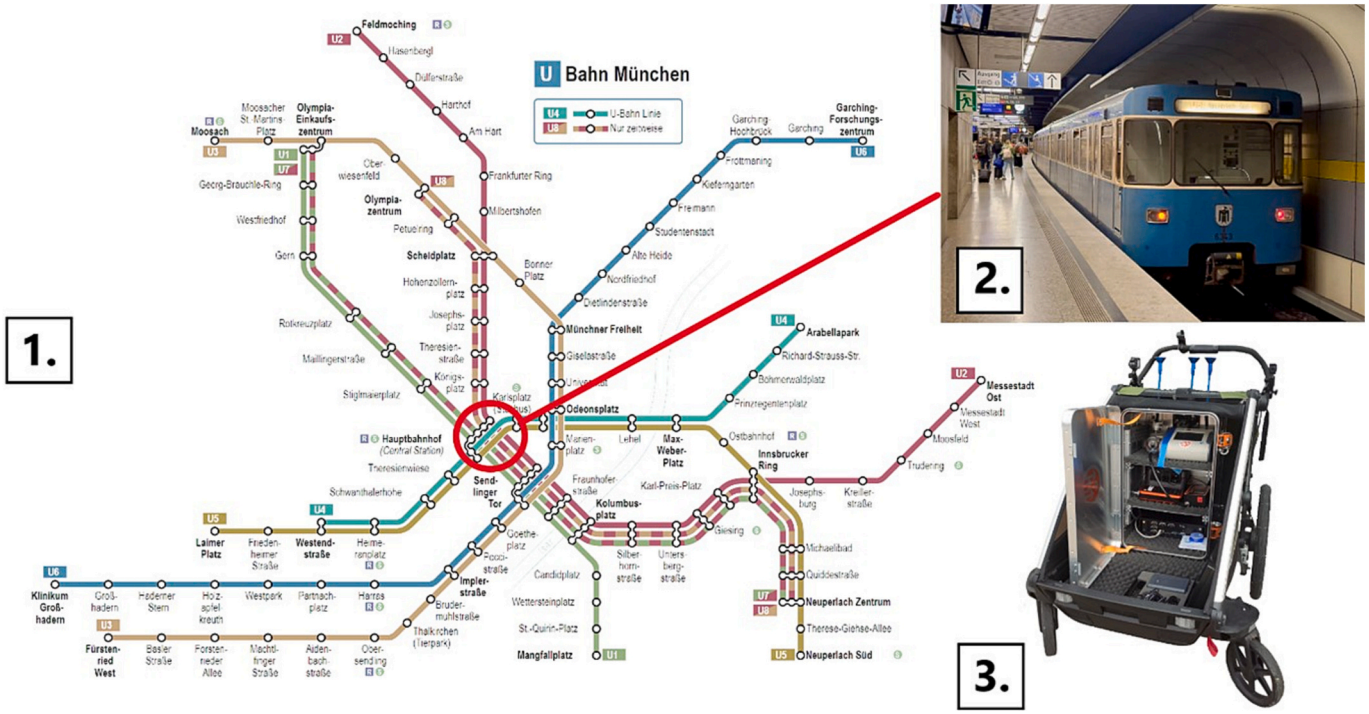

Fig. 1. Studied area and mobile measurement system. 1. Map of the Munich subway system (Wikipedia, 2023) 2. Platform of U4/U5 at the Munich central station (U-Bahn München, 2023b) 3. Mobile measurement system used in this study.

electrons to optimize the analysis for particles sizes well below 1 μm. At 15 kV the UltimMax 170 and at 5 kV the UltimExtreme was used to collect the X-Ray data. Measurements with 15 kV were conducted with a 2 nA beam current. Image acquisition settings were chosen so that 1 μm sized particles are described by at least 5 pixels. The smallest particles measured are 770 nm in diameter (ECD), which corresponds to 3 pixels in the image. EDX Spectra were acquired for 0.3 s per particle, which results in approximately 40.000 counts. Measurements with 5 kV were also conducted with a 2 nA beam current. Image acquisition settings were chosen so that 200 nm sized particles, which is also the smallest particle size that was measured, are described by at least 5 pixels. The EDX spectra were acquired for 2 s per particle, which results in approximately 200,000 counts. The longer acquisition was chosen to measure a significant number of X-rays coming from the small particles. The overlap in particle counts from 770 nm to 1 μm for filter measurements at 15 kV and 5 kV was manually deleted from the 15 kV dataset to avoid double counting of particles. The overlapping size region was measured intentionally for normalization between the rates of automated particle recognition, later used for compiling size distributions.

The classification scheme was built and developed based on a modified version of the technical cleanliness scheme provided by Oxford Instruments GmbH. To address the differences between carbon coated particles on filters and particles on silica wafers, as well as differences due to particle sizes, three different versions of the scheme were developed. Table S3 and Table S4 in the supplementary information (SI) list the boundaries and rulesets for each class of the three schemes. Classes were established based on a thorough scan of literature, to represent the particle types that can be expected in the subway environment, such as iron oxides and copper particles. Several classes like the critical fibers class, which scans for asbestos like fibers and the geological origin class scanning for silicates, salts and carbonates, were also established since these classes are of general interest to public health or offer insight into the interaction between the outside world and the subway environment. In total 10 main classes were defined during this stage, which were later divided into 31 subclasses, to allow for a more accurate distinction. For example, the brake wear class was subdivided into the two classes barium sulfate ($BaSO_4$) and antimony trisulphide (SbS_3), since these are common additives used in the manufacturing of brake pads (Grigoratos and Martini, 2015). Finally, three rejection classes were integrated into the scheme to discard particles larger than the investigated size range of a sample (only 5 kV measurements on filters) and artifacts caused from sample preparation, such as scratches in the wafer structure and particles from the conductive silver paint (only wafer measurements).

Morphological descriptors such as the particles maximum (X_{Fmax}) and minimum (X_{Fmin}) feret diameter, area A, perimeter p and dynamic shape factor x were directly obtained from the ZEN core and AZtec Features Software, while other parameters, such as the equivalent perimeter diameter (EPD), aspect ratio (AR), extent bulkiness, compactness, circularity, roundness and solidity were calculated based on Eqs. (1) to (8) from the ISO 21363:2020. These values can be used to address a particles shape, giving a numeric value that can be directly compared to other particles.

$$ECD = \sqrt{\frac{4\,A}{\pi}} \tag{1}$$

$$EPD = \frac{p}{\pi} \tag{2}$$

$$AR = \frac{x_{Fmin}}{x_{Fmax}} \tag{3}$$

$$extent\ bulkiness = \frac{A}{x_{Fmin}\ x_{Fmax}} \tag{4}$$

$$compactness = \frac{\sqrt{\frac{4\,A}{\pi}}}{x_{Fmax}} \tag{5}$$

$$circularity = \frac{ECD}{EPD} = \sqrt{\frac{4\,\pi\,A}{p^2}} \tag{6}$$

$$roundness = compactness^2 \tag{7}$$

The Zen core software additionally calculated the so-called convex hull, which is the smallest convex set containing a given geometric object. With this data the solidity and the convexity of particles were calculated, given the Eqs. (8) and (9) with the area of the convex hull A_C and the perimeter of the convex hull P_C.

$$solidity = \frac{A}{A_C} \tag{8}$$

$$convexity = \frac{P_C}{P} \tag{9}$$

Furthermore, the equivalent aerodynamic diameter D_A was calculated based on the ECD, the particle density p_p and the particles dynamic shape factor via Eq. (8) given by Hinds (Hinds and Zhu, 2022). This value is commonly used in aerosol research and allows for a direct comparison of particle size data measured via a SEM to data obtained from other devices such as an OPS.

$$D_A = ECD\ \sqrt{\frac{p_p}{p_0\ x}} \tag{10}$$

For particles measured via the ZEN core software, additional data regarding the legendre ellipse was also recorded. The legendre ellipse is an ellipse with the centre in the object's centroid and with the same geometrical moments up to the second order as the original object area (Besterci et al., 2001). These values were used to calculate the ellipticity, elongation and dispersion of particles according to Eqs. (11) and (12) provided by Besterci (Besterci et al., 2001), where a is the semi-mayor and b the semi-minor of the legendre ellipse.

$$ellipticity = \frac{a}{b} \tag{11}$$

$$elongation = log_2\left(\frac{a}{b}\right) \tag{12}$$

Table S1 in the SI shows an overview of the shape describing morphological features for different particle shapes to give a better understanding of the meaning of each parameter. Morphological data was acquired utilizing the extended particle analyzer feature from the BioVoxxel plugin (Brocher, 2022) via the ImageJ image analysis software. These morphological descriptors address a variety of parameters that are relevant for the characterization of particle morphology. Descriptors like the AR, ellipticity, extent bulkiness as well as the compactness and the roundness give a general understanding of the form of a particle, while other parameters like the solidity and the circularity describe the surface of a particle.

3. Results and discussion

3.1. Online measurements & gravimetric analysis

The online data obtained from stationary platform measurements are listed in Table 1. In summary, PM and PNC concentrations were comparable for all three samples at the Hauptbahnhof U4/U5 platform, despite the different sampling times. As discussed in our previous study (Bendl et al., 2023), the PNC were similar to ambient background levels at our suburban reference station located on the University campus (*GPS: 48°04'37.5"N 11°38'21.2"E)* and its vicinity using walking measurements. This observation, coupled with the absence of active

Table 1
Online data from platform stationary measurements obtained via OPC and DISCmini.

Date	PM in μg m^{-3}			PNC in $\#/cm^{-3}$	size mode in nm
	PM_{10}	$PM_{2.5}$	PM_1		
17/5/2022	231 ± 52	96 ± 10	25 ± 3	6099 ± 630	56 ± 3
19/7/2022	218 ± 50	85 ± 8	26 ± 2	7857 ± 713	54 ± 3
28/8/2022	181 ± 32	105 ± 24	29 ± 5	5074 ± 1111	64 ± 7

ventilation in the Munich subway system, and the location of the surveyed subway platform in the city centre with substantial traffic, leads us to conclude that the air exchange rate with the ambient air is relatively low. This aligns with the findings of Kumar et al., 2023, and suggest a low influence of traffic-related particles. The subway was identified as a dominant source of PM on the platform, with high concentrations of coarse particles. While the size mode of the PNC was outside of the range measured via the automated SEM/EDX approach, the data from DISCmini showed that there was no noticeable increase in the ultrafine fraction when entering the Munich subway system (Bendl et al., 2023). Overall PM levels on the platform were relatively stable over the sampling period suggesting that the samples were representative. Only small fluctuations in concentrations were observed, while short term $PM_{2.5}$ and PM_{10} peaks were associated with particle resuspension caused by incoming trains and piston effects (Bendl et al., 2023).

Simultaneous sampling for gravimetric analysis was performed on PC, PTFE and quartz filters and the $PM_{2.5}$ mass concentrations were 100.2 ± 4.13, 103.2 ± 1.65 and 102.9 ± 5.66 μg m^{-3}. Based on the comparison between gravimetry and on-line measurements, the average $PM_{2.5}$ effective density was estimated to be 2.1 g cm^{-3}, which was used as a correction factor for on-line PM data. This gravimetric approach also confirmed that $PM_{2.5}$ collection on PC filters is comparable to quartz and PTFE filters (Bendl et al., 2023).

3.2. SEM/EDX analysis

High resolution automated morphological measurements on PC filters conducted via Zen core listed particles predominantly in the submicron size, with the mode of the particle number between 200 and 300 nm, with similar distributions for the three different days. The size distribution from the 19/7/2022 measured via ZEN core as well as the size distribution of the iron oxides measured via AZtec Features and the online OPS size distribution for the same day are plotted in Fig. 2. Since automated imaging generally provides a value with the unit number or number per area, while online measurements yield results with the unit number per volume, these values were normalized to allow for comparison of these size distributions by normalizing the peak of each distribution to the value of 1. Size distributions of overall particles showed a similar trend as the size distributions of iron oxide particles, with a noticeable deviation around 1 μm where the transition between the two automated SEM/EDX measurement sizes occurred and can most likely be attributed to the different signal responses and, therefore, different rates of recognized particles for measurements at 5 kV and 15 kV. The online OPS size distribution showed the mode of particles at 300–400 nm and differed to the other distributions, most likely due to the lowered counting efficiency of laser scattering based instruments at lower particle sizes (Heim et al., 2008) and the lowest measurable size of 300 nm with the used instrument.

The dataset showed that the majority of particles was still in the size range measurable via automated SEM/EDX imaging, thus proving the validity of classification data for the Munich subway system. Manual EDX analysis furthermore confirmed that there were no apparent differences in elemental composition between small particles compared to particles above the set threshold for automated SEM/EDX analysis of 200 nm. Even though the online PNC size mode was found around 50 nm, there was no significant increase of PNC concentrations inside and outside of the subway system (Bendl et al., 2023), suggesting that the subway system does not produce copious amounts of ultrafine particles.

Particle shapes revealed an elongation of particles, which is expressed by their average aspect ratios of 0.66 ± 0.13 (17/5/2022 and 28/8/2022) and 0.65 ± 0.13 (19/7/2022) as well as their roundness of 0.55 ± 0.14 (17/5/2022 and 19/7/2022) and 0.56 ± 0.13 (28/8/2022). These values are further supported by the results for the legendre ellipse, which showed an average elongation of 0.68 ± 0.41 (17/5/2022), 0.69 ± 0.40 (19/7/2022) and 0.66 ± 0.39 (28/8/2022) and an ellipticity of 0.65 ± 0.16 (17/5/2022 and 28/8/2022) and 0.64 ± 0.16 (19/7/2022). The surfaces of analyzed particles were mainly rough with a largely increased surface area generally attributed to formation via abrasion processes. The roughness of particle surfaces is expressed by their average circularity of 0.78 ± 0.12 (17/5/2022), 0.79 ± 0.11 (19/7/2022) and 0.81 ± 0.10 (28/8/2022) as well as the solidity of 0.87 ± 0.08 (17/5/2022), 0.88 ± 0.07 (19/7/2022), and 0.88 ± 0.06 (28/8/2022). Table 2 summarizes the morphological data for subway particles on PC filters measured via ZEN core. Overall morphological data showed high intra-sample variance with almost no inter-sample variance suggesting that different modes of particles are generated from the same source with little seasonal influence. Considering that indoor environments are less susceptible to weather and temperature changes the neglectable seasonal variance that was observed between samples can be considered as reasonable.

Automated SEM/EDX based imaging of subway aerosols classified the majority of particles as iron rich particulate matter (FePM). The initial classification, however, contained several artifacts originating mainly from scratches in the surface of the silica wafers and from the pores of the filters. A manual correction of the dataset was therefore conducted, where particles that had no elemental data associated to them were deleted. Initial results showed average values of unclassified particles at 3.29 ± 3.77 % for the three wafer samples (W15), 0.71 ± 0.22 % for the three filter samples measured at 15 kV (F15), and 11.74 ± 4.21 % for the fine particle fraction <1 μm of the same filter samples measured at 5 kV (F5), which was lowered via manual data cleanup to 0.24 ± 0.05 % (F15), 1.86 ± 1.36 % (W15) and 1.30 ± 0.45 % (F5). Fig. 2 shows the average percentages of the assigned classes for all three F15 samples. Further diagrams of the average classification percentages for F5 and W15 samples can be found in the SI in Fig. S3 and Fig. S4 together with Table S2, which shows the number of particles found in each sample. Standard deviations shown for percentages of particle classification indicate the variance between the three sampling days.

In total, 92.78 ± 1.05 % of all particles (F15) were assigned to the iron oxide class, while 4.28 ± 1.49 % belonged to the three steel subclasses resulting in a total of 97.06 ± 0.64 % of iron-rich particles. The average iron oxide percentage for W15 samples was slightly lower at 84.93 ± 5.48 % with an additional 8.75 ± 2.23 % of steel particles totaling at 93.68 ± 3.28 % of iron-rich particles. The differences between these two sample types can be explained by the usage of two different classification schemes that were applied to the samples, which included Si percentages for the filter samples and C percentages for the wafer samples resulting in particles falling below, or exceeding a certain class threshold. F5 samples consisted of a total of 63.30 ± 10.47 % of iron-rich particles, with 62.69 ± 10.16 % of all particles classified as iron-oxides and only 0.61 ± 0.32 % of steel particles. F5 samples showed a large amount of iron bearing particles in the submicron size range, however, the results were significantly lower than for particles ≥1 μm in diameter (F15 samples), which is due to the higher number of carbonaceous particles in these samples. Zhang et al. (2022) stated that iron was found in >75 % of particles (90 particles per sample) in Beijing, China, while Jung et al. (2010) reported that 75–91 % of all analyzed subway particles (300 particles per sample) in Seoul, South Korea were

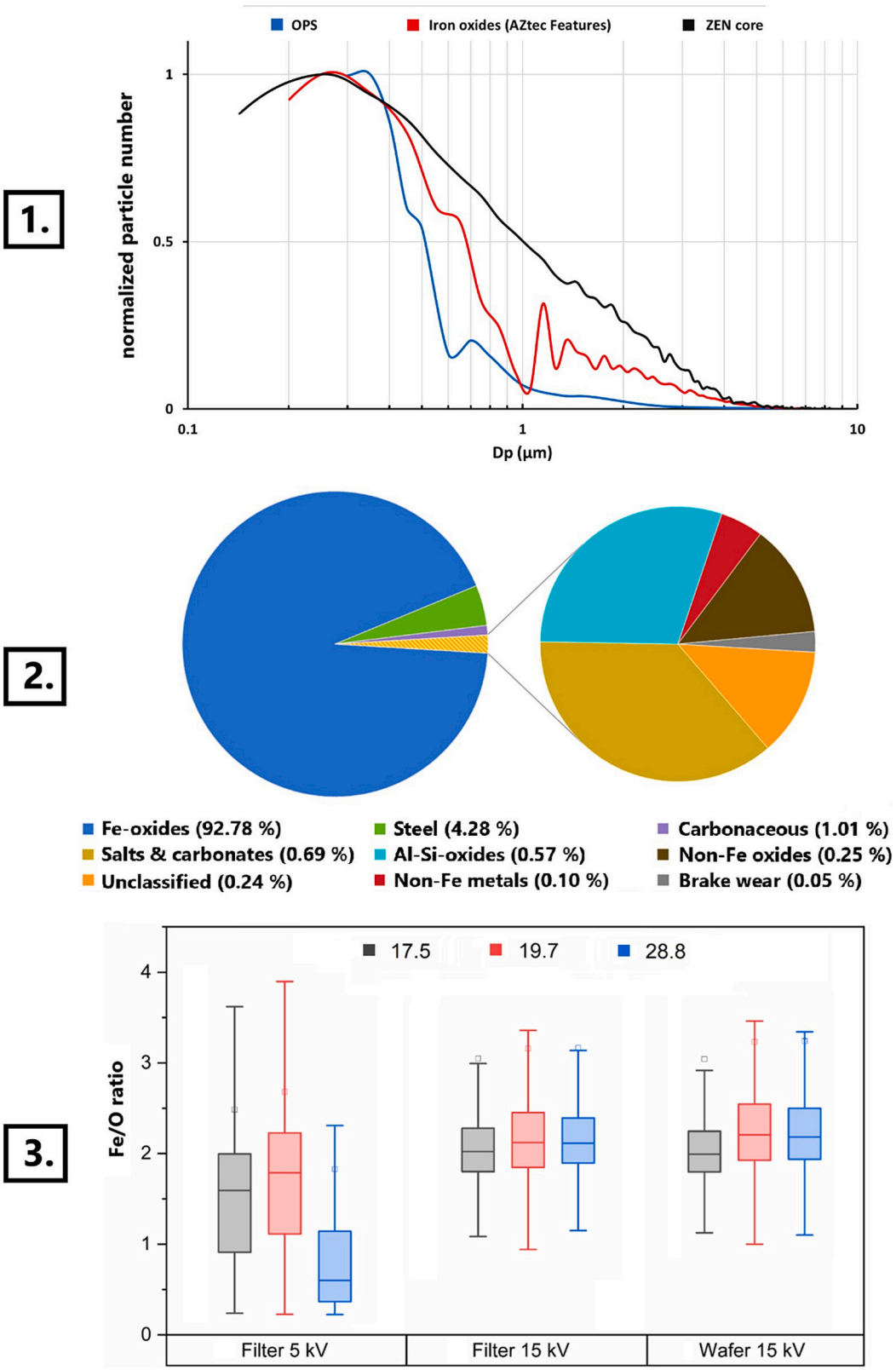

Fig. 2. Statistical information obtained via automated imaging. 1. Size distributions of particles from 19/07/2022 measured via ZEN core, iron oxides measured via Aztec Features and online size distribution obtained by OPS. Highest numbers for size bins were normalized to 1 for easier comparison of different techniques. 2. Average classification results of particles larger than 1 µm for filter samples measured at 15 kV. 3. Fe/O ratios of particles classified as iron oxides.

Table 2
Morphological descriptors for subway particles on filter samples measured via the ZEN core Software.

Descriptor	17/5/2022			19/7/2022			28/8/2022		
Particle count	45,640			68,447			87,287		
AR	0.66	±	0.13	0.65	±	0.13	0.66	±	0.13
Extent bulkiness	0.66	±	0.07	0.66	±	0.07	0.67	±	0.06
Compactness	0.74	±	0.10	0.74	±	0.09	0.75	±	0.09
Circularity	0.78	±	0.12	0.79	±	0.11	0.81	±	0.10
Roundness	0.55	±	0.14	0.55	±	0.14	0.56	±	0.13
Solidity	0.87	±	0.08	0.88	±	0.07	0.88	±	0.06
Convexity	0.90	±	0.08	0.91	±	0.08	0.92	±	0.07
Ellipticity	0.65	±	0.16	0.64	±	0.16	0.65	±	0.16
Elongation	0.68	±	0.41	0.69	±	0.40	0.66	±	0.39

iron-rich. Higher percentages of FePM in the Munich subway can be explained by the lower proportion of Cu rich particles due to the usage of a third-rail type power supply, instead of a copper catenary and the comparably low part of geological/ soil derived particles caused by the depth of the subway station at which samples were drawn and lower air exchange with the ambient air. These results suggest a similar origin of iron rich particles in the subway systems all over the world.

Fig. 3 contains six SEM micrographs of typical iron oxide particles found in the Munich subway system showcasing their overall form and surface topography. Fig. 3.1 and Fig. 3.3 depict flake like iron-oxide particles, which were commonly found throughout all samples, predominantly for particles >2 μm. Iron oxide particles exhibited rough and often splintery shapes with large surface areas due to the jagged edges often found on abrasion derived particles. This is expressed by their

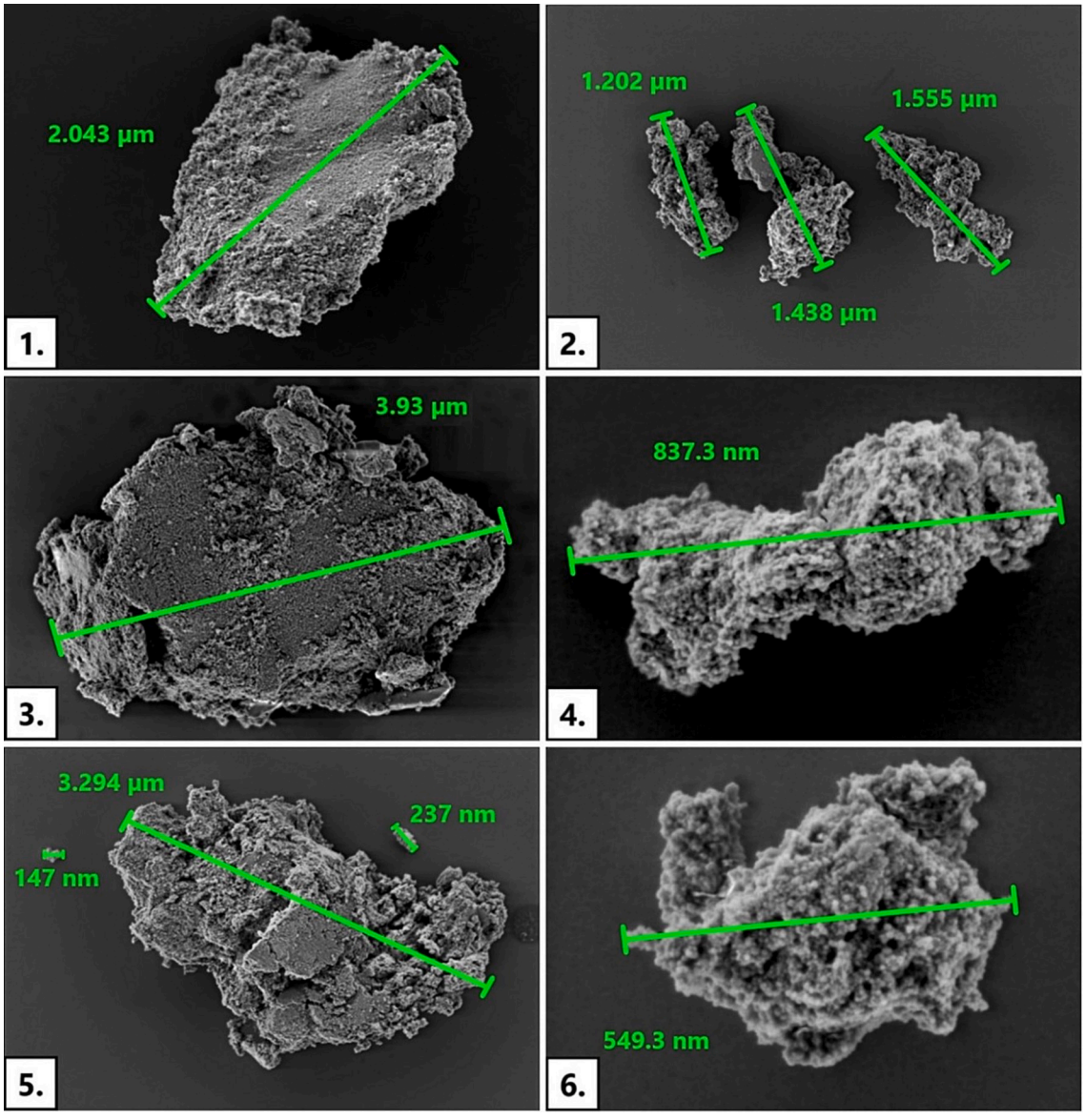

Fig. 3. SEM micrographs of characteristic iron oxide particles found in the Munich subway system.

circularity of 0.87 ± 0.12 (F15 and W15), and 0.88 ± 0.11 (F5). However, due to the comparably low magnification used for automated SEM/EDX imaging, an underestimation of particles perimeter is likely due to the limited number of pixels describing a particle. This is in accordance with the significantly lower circularity of all particle classes of 0.80 ± 0.11 determined with Zen core, which utilized a higher magnification for measurements. Since almost all particles found were classified as iron-oxide particles, the value obtained via ZEN core can be regarded as more probable.

The average aspect ratios for iron oxide particles were 0.62 ± 0.13 (F15), 0.60 ± 0.13 (W15), and 0.63 ± 0.12 (F5) indicating an elongation of particles, which is visible in Fig. 3.2 and Fig. 3.4 as splintery particles, mainly found in the <2 μm size range. This fact is also represented by the average roundness of iron oxide particles of 0.46 ± 0.11 for particles >1 μm and 0.49 ± 0.11 for particles <1 μm as well as an extent bulkiness of 0.60 ± 0.10 (F15), 0.61 ± 0.10 (W15), and 0.62 ± 0.09 (F5). Iron oxide particles were found in a fine mode at 484 ± 198 nm and a coarse mode at 1534 ± 1024 nm (W15) and 1853 ± 796 nm (F15). Morphological descriptors for iron oxide particles are summarized in Table 3.

Particles classified as iron oxides consisted almost exclusively of iron and oxygen with 14.13 ± 4.51 wt% of carbon (based on wafer samples) and 0.8 ± 1.31 wt% (F15) to 4.39 ± 2.67 wt% (F5) of Si. Other elements, mostly S, Cu, Na, Ca, Mg, Al and K, were also detected, but only at average concentrations below 0.2 wt% for individual elements. These values are in good agreement with data from Kumar et al. (2023) and Moreno et al. (2015) who reported elemental compositions for iron rich particles of 40.16–64.69 wt% for Fe, 9.08–32.47 wt% for O, 1.96–19.52 wt% for C, and 1.05–8.47 wt% for Si. Table 4 shows the average elemental composition of iron oxide particles for the three sample types. Furthermore the data obtained via SEM/EDX is in good agreement with results published in our previous study (Bendl et al., 2023) obtained via ICP-MS for the same days, which showed iron concentrations accounting for up to 69 wt% of the $PM_{2.5}$ fraction for the 17/5/2022.

The high average carbon percentages found in iron oxide particles suggests that most of these particles originated from brake pads instead of a low steel source, which would be attributed to the rails and wheels as well as the third rail power conductor (Font et al., 2019; U-Bahn München, 2023a). The high oxygen contents, which align neither with the chemical composition of cast iron nor with steel, can be explained by the high temperatures at the brake during particle formation facilitating rapid oxidation in the environment (Wang et al., 2016). Fe/O ratios of iron oxide particles <1 μm were less uniform than for those >1 μm indicating a wider spread of oxidation levels in the submicron size range. The average Fe/O ratio for small iron oxide particles was lower than for larger iron oxide particles, which is presumably linked to their higher surface area rendering them more susceptible to oxidation, while the fraction of the oxidized surface layer in comparison to the unoxidized Fe core also increases. Furthermore, there might be a slight underestimation of iron contents in small particles due to the lower EHT of 5 kV limiting the quantification of iron to the Lα line instead of the more accurate Kα line. Fig. 2 shows the Fe/O ratios for iron oxide particles for all sample types.

Metallic iron and steel particles, which also held a high share of subway particles at percentages between 0.61 and 8.75 % of all particles, where especially present in W15 samples. Filter samples consisted almost exclusively of low alloy steel and metallic iron particles with 99.77 ± 0.01 % (F15) and 100.00 % (F5), which is due to the less accurate distinction between steel types without measured carbon contents for these samples. The average D_A of steel particles in W15 samples was 2146 ± 1287 nm with a distribution of 94.50 ± 1.84 % of low alloy steel and metallic iron, 4.78 ± 1.82 of high alloy steel, and 0.72 ± 0.26 % of Cr-steel. These steel particles are attributed to abrasion of train wheels and rails (Moreno et al., 2015), which are commonly made of R260 or similar steel types (Aniołek and Herian, 2011).

While automated SEM/EDX analysis classified the majority of particles >200 nm as iron rich, even smaller particles of highly ferrous nature were present in the samples. Manual SEM/EDX analysis also revealed iron concentrations of similar levels compared to >200 nm subway particles in NPs ranging from 30 nm to 200 nm. Concentrations obtained from these measurements, which were obtained at 5 kV, are less accurate due to the beam partially piercing the particle and subsequently exciting the underlying filter or wafer. Nonetheless, based on a simulation of the penetration depth of electrons in a Fe_2O_3 substrate at an EHT of 5 kV calculated via the Monte Carlo software (Fig. S1 and Fig. S2 in SI), they can be considered reliable enough to give an estimation of the elemental composition of particles <200 nm. From a toxicologic viewpoint these particles, especially those NP in the sub 100 nm range, are considered to be critical due to their ability to reach the bloodstream via deposition in the alveoli followed by translocation throughout the whole body (Morawska and Buonanno, 2021; Thorley et al., 2014). Additionally, NPs were reported to be transported across the olfactory epithelium leading to accumulation in the brain (Hopkins et al., 2018; T. Fortoul et al., 2015). Fig. 4 shows a 68 nm iron oxide particle with its corresponding EDX spectrum as well as other small heavy metal rich particles found in the samples.

FePM is generally considered less toxic than particles containing other heavy metals such as Cu, however, FePM was shown to significantly impair human health following inhalation in several studies (Beck-Speier et al., 2009; Lay et al., 1999). While Fe can be generally considered as innocuous if ingested orally due to bounding of iron to proteins and chelating in the digestive system that prevent the generation of ROS (Morgan et al., 2020), the lung does not possess a pathway for coping with large amounts of unliganded ferrous or ferric iron (Ghio et al., 2009). Carcinogenic potential of long-term exposure to low-dose Fe_2O_3 nanoparticles resulting in neoplastic-like transformation of human small airway epithelial cells via formation of ROS was reported by Stueckle et al. (2017) emphasizing the significance of sub 100 nm iron rich particles in the subway, to which commuters are exposed on a daily base. Furthermore, particles formed by physical abrasion, mainly grinding and crushing, are suggested to exhibit significantly different toxicological responses compared to combustion derived Fe particles, such as fly ash, due to their rough, often flake like shape (Morgan et al., 2020). Generation of ROS from heavy metals via Fenton-like reactions requires the metal proportion of particles to be soluble putting a large significance on bioavailability of heavy metal rich PM (Longo et al., 2016; Zhang et al., 2008). Increased toxicity for subway FePM was reported in several studies (Jung et al., 2012; Loxham and

Table 3
Morphological descriptors for iron oxide particles obtained via the Aztec Features software.

Descriptor	Wafer 15 kV			Filter 15 kV			Filter 5 kV		
ECD in nm	1534	±	1024	1853	±	796	484	±	198
EPD in nm	1936	±	1813	2256	±	1380	572	±	288
D_A in nm	1832	±	976	2200	±	808	606	±	230
AR	0.60	±	0.13	0.62	±	0.13	0.63	±	0.12
extent bulkiness	0.61	±	0.10	0.60	±	0.10	0.62	±	0.09
compactness	0.67	±	0.09	0.67	±	0.09	0.70	±	0.08
circularity	0.87	±	0.12	0.87	±	0.12	0.88	±	0.11
roundness	0.46	±	0.11	0.46	±	0.11	0.49	±	0.11

Table 4
Average elemental compositions of iron oxides for filter and wafer samples.

Element	Wt% for Filter 15 kV			Wt% for Wafer 15 kV			Wt% for Filter 5 kV		
C	ND			14.13	±	4.51	ND		
O	32.58	±	6.00	27.37	±	3.17	45.53	±	13.06
Si	0.80	±	1.31	ND			4.39	±	2.67
Fe	66.30	±	6.88	58.13	±	6.63	49.58	±	14.14
Other elements	1.12	±	5.32	0.36	±	3.10	4.88	±	6.46

Nieuwenhuijsen, 2019) with a twofold increase in DNA damage compared to Fe_2O_3 or Fe_3O_4 particles alone (Karlsson et al., 2008). An investigation of various PM sources including wood combustion, tyre wear, street PM and subway particles conducted by Karlsson et al. (2006) showed subway aerosol as the most genotoxic with significantly increased DNA damage, which cannot solely be explained by enlarged surface areas, but was attributed by them to a highly reactive surface of these particles. Additionally, iron rich PM is often accompanied by other heavy metals, such as Cu, Mn, Cr and V, further enhancing its potential to generate ROS compared to pure iron and iron oxide particles. Furthermore, the small clearance between trains and the tunnel walls leads to resuspension of sedimented particles via the so called "piston-effect", which can temporarily cause high particle concentrations in the surrounding air by pushing the air in front of the trains and creating a strong suction behind them (Walther and Bogdan, 2017). These short-term exposures to high PM concentrations might be reduced in the Munich subway system compared to other cities, by the usage of a specialized vacuum train called "VakTrak, which is used to clean the track bed from waste and debris and filters out resuspended particles down to 100 nm (Trambahn.de, 2023). Additionally, the Munich transport network (MVG) operating the subway is planning the installation of platform screen doors in the future (mvg.de, 2023), which some studies showed to mitigate commuters' exposure (Kim et al., 2012; Son et al., 2013).

While these iron oxide and steel particles are well reported in the literature and are linked to abrasion at the rail-wheel-brake interface (Moreno et al., 2015) other distinct chemical profiles linked to the emission of subway trains were only scarcely found. Except from iron oxide and steel particles, the third most abundant class was carbonaceous particles present at concentrations of 1.01 ± 0.15 % (F15), 23.62 ± 14.61 % (F5), and 2.35 ± 1.62 % (W15). While carbonaceous particles are normally related to automotive traffic, only minor amounts of soot chains, typical for the incomplete combustion of fuels, were found in all samples. Instead, carbonaceous particles were almost exclusively found in the submicron size range with an average aerodynamic diameter of 385 ± 136 nm, but also to some degree in the size range of 1388 ± 804 nm (W15) to 1641 ± 354 nm (F15). Automated classification of carbonaceous particles, however, is only accurate for Wafer samples since no carbon was measured in filter samples and the classification was based on the assumption that particles consisting of >75 wt% of O have to be carbonaceous in order to be solid, since all other elements except C were measured. Furthermore, manual EDX measurements confirmed that these particles were in fact carbonaceous and present in high quantities, even though their carbon content could not be accurately quantified. The small fraction of carbonaceous particles (F5) showed similar morphological characteristics as iron oxide (Yang et al., 2016) particles with an average roundness of 0.43 ± 0.12 and a circularity of 0.84 ± 0.13. These values indicate a similar, abrasion derived source, possibly generated from frictional wear of graphite contact blocks used in the current collectors of third-rail type power supplies (Yang et al., 2016) or from other sources, such as electric motor brushes employed in newer trains as well as brake pads (Moreno et al., 2015).

Font (Font et al., 2019) analyzed motor brushes used in the Barcelona subway system, which showed Zn, Ti, Ba, Sn, and Cr as the main impurities of the carbon nanotubes, which are employed in these brushes. Carbonaceous particles in F5 samples contained 7.53 ± 5.21 wt % of Fe and 0.27 ± 0.51 wt% of Cu with no other metal concentrations above the limit of detection for EDX analysis. This elemental composition, even though actual values are most likely lower due to the missing carbon content in these samples, contradicts motor brushes as main source of carbonaceous particles in the Munich subway environment and points towards brake wear as the most likely source. The fact that submicronic carbonaceous particles contained iron and copper also renders the assumption that these particles might be artifacts from the sputtering process improbable. The F5 sample from the 28.8 showed especially high amounts of carbonaceous particles in the submicron fraction indicating a high temporal variability of these particles with a total range of 10.31 % (19.7) to 43.97 % (28.8).

Heavy metal bearing particles, linked to wear and abrasion of brake pads, such as $BaSO_4$ and SbS_3 (Grigoratos and Martini, 2015), were also present at concentrations of 0.05 ± 0.01 % at an average size of 2286 ± 936 nm (F15) and 0.09 ± 0.05 % at an average size of 1459 ± 416 nm (W15). F5 samples did not show significant amounts of brake wear particles due to the general lack of Sb rich particles in all subway samples and the insufficient EHT to excite the Lα line of the more frequently occurring Ba. Since the M-line of Ba, which can be observed at an EHT of 5 kV, is overlapping with the L-Lines of Fe, it could not be used for determination of Ba presence due to the ubiquitous nature of Fe in the subway environment. Abbasi et al. (2012) reported peaks for railway break wear in the ultra-fine size range at around 100 nm; two fine peaks - one dominant at 300–400 nm and one at 500–600 nm - and a coarse peak at 3–7 μm, which were found under all test conditions. In contrast, Hagino et al. (2016) showed the coarse peak in the range of 1.2–3.5 μm. Furthermore, Iijima et al. (2007) showed that heavy metals associated to brake wear are predominantly found in the coarse fraction. This is in good accordance with data from the Munich subway, which showed the carbonaceous fraction of brake wear at 385 ± 136 nm and the heavy metal rich brake wear fraction in the coarse mode between 1459 ± 416 nm – 2286 ± 936 nm.

Average heavy metal concentrations, except for iron were present at low levels, however, they were found to be distributed inhomogeneously throughout the samples. Fig. 5 depicts an EDX map of the F15 sample from 28/8/2022 illustrating the distribution of metals such as Cu and Al.

Classification results listed non-ferrous metal rich particles at percentages of 0.10 ± 0.01 % (F15), 0.14 ± 0.07 % (F5) and 0.90 ± 0.30 % (W15) for the non-ferrous metals and 0.25 ± 0.15 % (F15), 2.00 ± 1.44 % (F5), and 0.09 ± 0.03 % (W15) for non-ferrous oxides. Most of these heavy metal containing particles were classified as metallic copper or copper oxide particles and are often attributed by literature to sparking at the catenary-pantograph interface, often consisting of Cu alloys (Zhou et al., 2022). However, these catenary-pantograph type power collectors are not utilized in the Munich subway. Wafer samples contained an average of 0.42 ± 0.02 % of copper rich particles, while filter samples contained at average 0.31 ± 0.14 % (F15) and 2.11 ± 1.52 % (F5). Samples taken on the 19/7/2022 showed significantly higher levels of Cu metal and oxide particles with Cu oxides reaching a level of 4.04 % in the F5 sample. These results show that while average numbers of Cu rich particles are fairly low, they can temporally reach high dosages, causing potential threads to commuters' health. Third-rail type power supplies, which are also used in the Munich subway, consists of either a graphite or a copper current collector (Yang et al., 2016) and might, therefore, contribute to copper rich emissions in subway tunnels. However, given

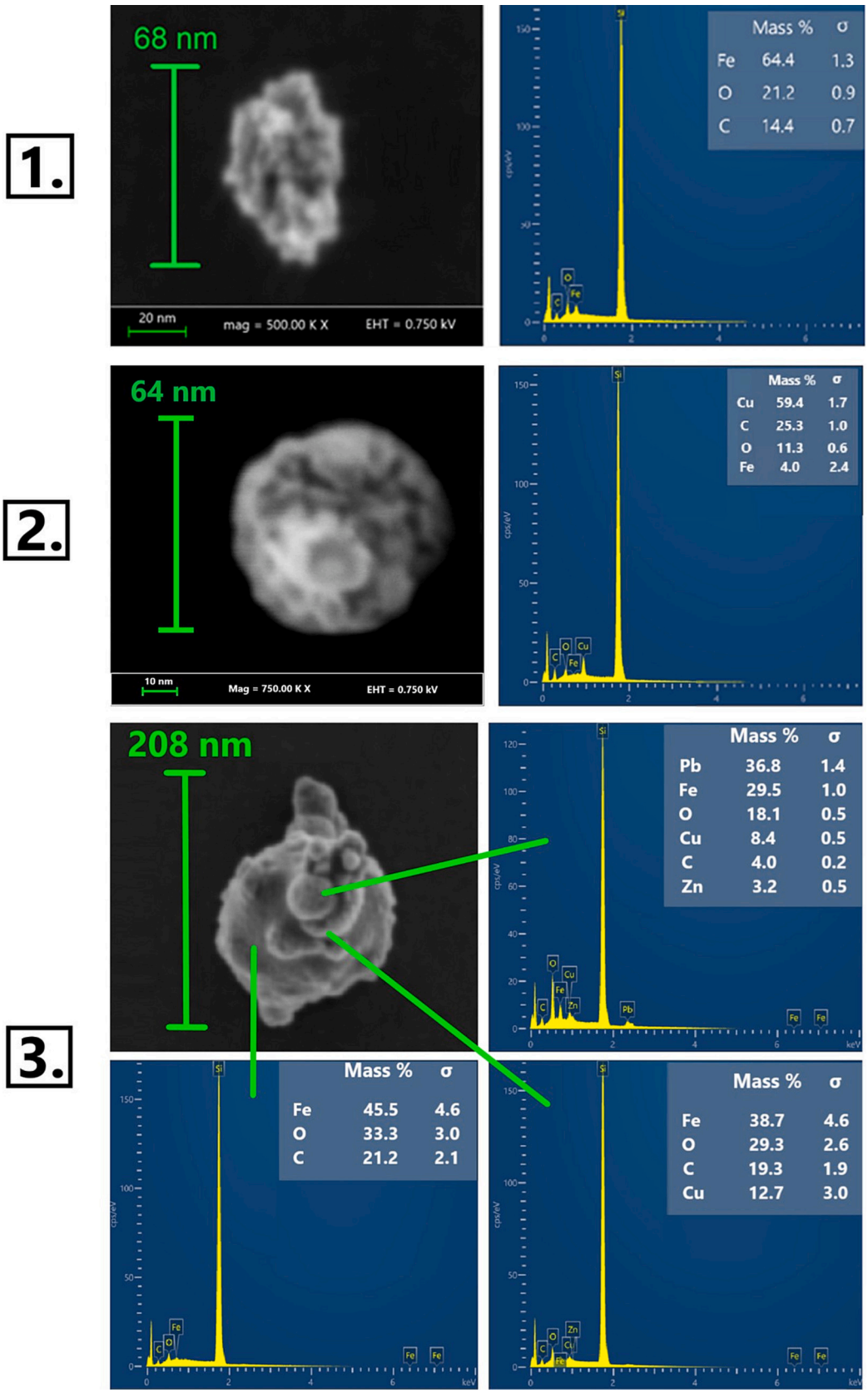

Fig. 4. Manual EDX data of small particles taken at 5 kV. 1. 68 nm iron oxide particle found in wafer sample from 28/8/2022. 2. 64 nm copper oxide particle found in wafer sample from 19/7/2022. 3. 208 nm iron oxide particle with Cu and Pb encrustations found in wafer sample from 28/8/2022.

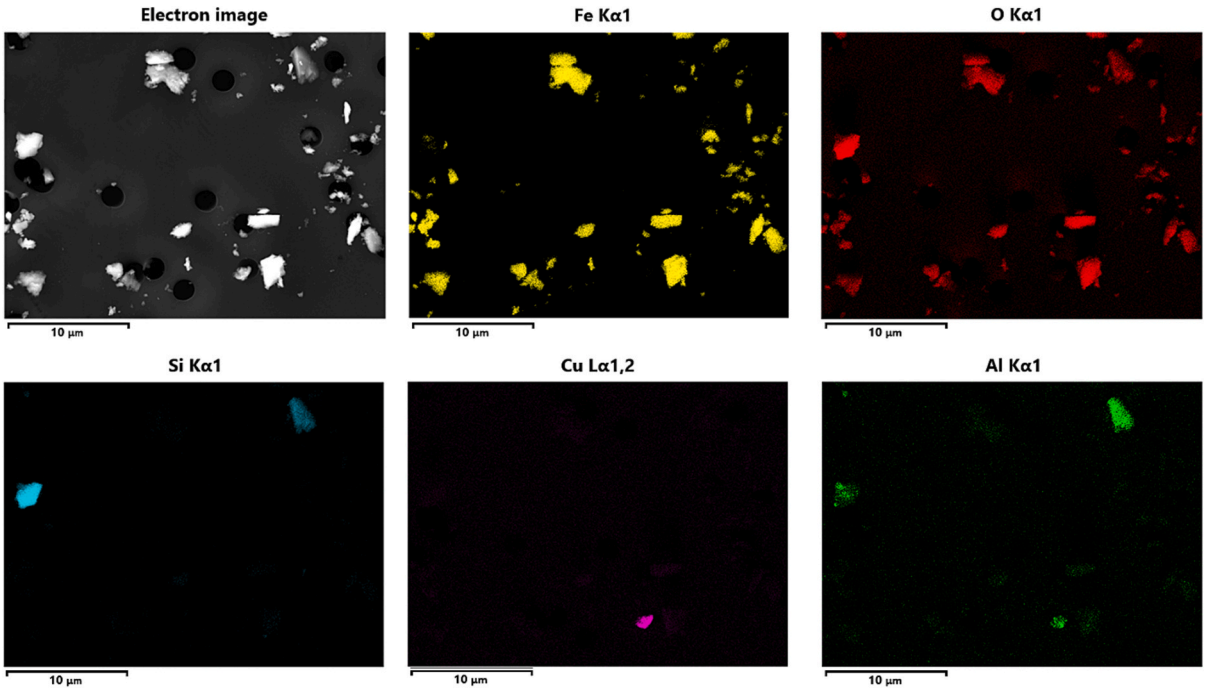

Fig. 5. EDX overview of sample from 28/8/2022 at 15 kV.

the low levels of copper in comparison to other subway systems (Bendl et al., 2023), it is likely that the current collectors are made of graphite, which is in good agreement with the high levels of carbonaceous particles found in the Munich subway system. These results point towards brake wear as the most likely source of copper in the subway tunnels, which is commonly used as marker for automotive brake wear (Grigoratos and Martini, 2015).

Cu particles found in the Munich subway system were found in two size modes. Cu particles in F15 and W15 samples had a particle size between 2029 ± 741 nm (F15) and 1432 ± 589 nm (W15) while the majority of Cu particles was found in F5 samples at an average particle size of 445 ± 191 nm. The average elemental compositions for the combined Cu oxides and Cu metal classes for all samples are given in Table S5 in the SI. These copper rich particles can be considered as critical to the human health since particles between 1 and 2.5 µm end up in terminal bronchi (Sankhe et al., 2019) and particles smaller 1 µm can even reach the pulmonary alveoli (Costa et al., 2016), where the generation of ROS can induce several diseases (Boukhenouna et al., 2018; Kanti Das et al., 2014). Especially temporary high concentrations, such as in the F5 sample from the 19/7/2022, where 4.04 % of all particles were copper rich, are critical considering that respirable copper particles are considered to be the most toxic heavy metal bearing particles in mammals (Hejazy et al., 2018). Fig. 4.2 contains a SEM micrograph of a 64 nm copper particle, together with its associated EDX spectrum highlighting the high mass percentages of copper that could be found even in particles smaller than 100 nm.

Apart from pure copper oxides, some iron-oxide particles were observed to contain encrustations of other heavy metals, such as Cu and Pb. An exemplary SEM micrograph of a 208 nm particle with its EDX spectra is shown in Fig. 4.3. For these particles, which contain a variety of heavy metals, the overall toxicity is hard to predict, however, studies suggest that the toxicity is higher than the sum of the toxicity of the individual heavy metals. Sun et al. reported that mixed heavy metals in $PM_{2.5}$ samples from smeltery districts in China showed an increased rate of apoptosis in A549 cells compared to the single metals (Sun et al., 2022).

Furthermore, non-anthropogenic sources of particles, mostly of geological origin, were observed in the Munich subway system. A total of 0.57 ± 0.07 % (F15) and 1.99 ± 0.66 % (F5) was assigned to silica, aluminosilicates and other various silicate types, while none were found in wafer samples, which is due to the fact that Si was excluded from these samples. These soil derived particles were presumably brought into the subway system by commuters or were transported to the platforms via ventilation from the streets above. The second most prominent detected non-anthropogenic particle source was the salts and carbonates class at 0.69 ± 0.24 % (F15), 0.77 ± 0.66 % (F5) and 0.97 ± 0.47 % (W15) dominated by calcium carbonate.

4. Conclusions

Automated SEM based morphological analysis of subway particles showed a high intra-sample variance, but almost no variance between samples, which were taken at the same place at different time and seasons suggesting the same dominant source, which is relatively stable over time. Particles found in the Munich subway system displayed rough edged splintery surfaces, indicated by their average circularity of 0.78 to 0.81, as well as an average solidity of 0.87 to 0.88. The main mode of the particle number was observed in the size range from 100 to 300 nm peaking at 175–200 nm. Two main types of particle morphologies, a flake like shape for particles >2 µm and an elongated shape for particles <2 µm, were predominantly found throughout all samples.

Of the over 200,000 particles analyzed via automated SEM/EDX imaging, 98.87 ± 1.06 % were automatically assigned to the pre-defined classes. Automated SEM/EDX based classification of the subway aerosol revealed the highly ferruginous nature of subway particles compliant with literature from other subway systems around the globe. In total, 84.68 ± 16.45 of all particles were found to be of iron rich nature with an average Fe concentration of these particles of 49.58–66.30 % depending on the particle size. Other heavy metals, mainly copper oxides, were found either as pure particles or as encrustations embedded into larger iron oxide particles. These high levels of Fe rich and other heavy metal bearing particles, which were also found in the size range well below 100 nm, could pose a threat especially to vulnerable groups, such as pregnant women and old and young people, if they are exposed to subway aerosol for prolonged periods of time.

These results highlight the desirability of reducing commuters'

exposure, for which other studies showed the installation of platform protection doors as one of the feasible mitigations. Another feasible mitigation to limit the exposure to short-term high particle concentrations due to the piston-effect might be improvement of the ventilation system and a more frequent removal of sedimented particles via specialized vacuum trains.

The suitability of automated SEM/EDX based imaging was demonstrated for the in-depth characterization of micro-environments, such as non-exhaust emissions. The technique described in this paper can be used to address the homogeneity of a wide variety of different emission sources, or to study their contribution to complex environmental samples. It can be used stand-alone or as a complement to other filter analysis techniques, such as ICP-MS, where the added value is mainly information on the distribution of elements in different particle sizes, which can have a major impact on health risks.

CRediT authorship contribution statement

Carsten Neukirchen: Writing – review & editing, Writing – original draft, Visualization, Investigation, Data curation, Conceptualization. **Thorsten Meiners:** Writing – review & editing, Writing – original draft, Validation, Software, Investigation, Data curation, Conceptualization. **Jan Bendl:** Writing – review & editing, Writing – original draft, Validation, Resources, Methodology, Investigation, Formal analysis, Data curation, Conceptualization. **Ralf Zimmermann:** Writing – review & editing, Writing – original draft, Validation, Supervision, Project administration, Funding acquisition. **Thomas Adam:** Writing – review & editing, Validation, Supervision, Resources, Project administration, Funding acquisition, Formal analysis, Conceptualization.

Declaration of competing interest

The authors declare that they have no known competing financial interests or personal relationships that could have appeared to influence the work reported in this paper.

Data availability

Data will be made available on request.

Acknowledgments

This research is funded by dtec.bw – Digitalization and Technology Research Center of the Bundeswehr [project LUKAS and MORE]. Dtec.bw is funded by the European Union – NextGenerationEU. This research was also supported by the project ULTRHAS – ULtrafine particles from TRansportation – Health Assessment of Sources, a project funded under the EU's Research and Innovation programme Horizon 2020, Grant Agreement No. 955390. We acknowledge financial support by Universität der Bundeswehr München.

Appendix A. Supplementary data

Supplementary data to this article can be found online at https://doi.org/10.1016/j.scitotenv.2024.170008.

References

2023 Netzplan U-Bahn München.svg – Wikipedia. https://de.m.wikipedia.org/wiki/Datei:Netzplan_U-Bahn_M%C3%BCnchen.svg (accessed 04 November 2023).

Abbasi, S., Jansson, A., Olander, L., Olofsson, U., Sellgren, U., 2012. A pin-on-disc study of the rate of airborne wear particle emissions from railway braking materials. Wear 284-285, 18–29. https://www.sciencedirect.com/science/article/pii/S0043164812000257.

Aniołek, K., Herian, J., 2011. The structure, properties and a resistance to abrasive wear of railway sections of steel with a different pearlite morphology. IOP Conf. Ser. Mater. Sci. Eng. 22 (1), 12012. https://doi.org/10.1088/1757-899X/22/1/012012.

Bachler, G., Losert, S., Umehara, Y., Goetz, N. von, Rodriguez-Lorenzo, L., Petri-Fink, A., et al., 2015. Translocation of gold nanoparticles across the lung epithelial tissue barrier: combining in vitro and in silico methods to substitute in vivo experiments. Part. Fibre Toxicol. 12 (1), 18. https://doi.org/10.1186/s12989-015-0090-8.

Beck-Speier, I., Kreyling, W.G., Maier, K.L., Dayal, N., Schladweiler, M.C., Mayer, P., et al., 2009. Soluble iron modulates iron oxide particle-induced inflammatory responses via prostaglandin E(2)synthesis: In vitro and in vivo studies. Part. Fibre Toxicol. 6, 34. https://doi.org/10.1186/1743-8977-6-34.

Bendl, J., Neukirchen, C., Mudan, A., Padoan, S., Zimmermann, R., Adam, T., 2023. Personal measurements and sampling of particulate matter in a subway – identification of hot-spots, spatio-temporal variability and sources of pollutants. Atmos. Environ. 308, 119883. https://www.sciencedirect.com/science/article/pii/S1352231023003096.

Besterci, M., Käerdi, H., Kulu, P., Mikli, V., 2001. Characterization of powder particle morphology. Proc. Estonian Acad. Sci. Eng. 7 (1), 22. https://doi.org/10.3176/eng.2001.1.03.

Boukhenouna, S., Wilson, M.A., Bahmed, K., Kosmider, B., 2018. Reactive oxygen species in chronic obstructive pulmonary disease. Oxidative Med. Cell. Longev. 2018, 5730395. https://www.hindawi.com/journals/omcl/2018/5730395/.

Brocher, 2022. biovoxxel/BioVoxxel-Toolbox: BioVoxxel Toolbox. Zenodo.

Čalkovský, M., Müller, E., Gerthsen, D., 2023. Quantitative analysis of backscattered-electron contrast in scanning electron microscopy. J. Microsc. 289 (1), 32–47. https://doi.org/10.1111/jmi.13148.

Costa, A., Pinheiro, M., Magalhães, J., Ribeiro, R., Seabra, V., Reis, S., et al., 2016. The formulation of nanomedicines for treating tuberculosis. Adv. Drug Deliv. Rev. 102, 102–115. https://doi.org/10.1016/j.addr.2016.04.012.

DB Netz AG, 2023. Stationsbau - 2. Stammstrecke München. https://www.2.stammstrecke-muenchen.de/stationsbau.html. (Accessed 15 September 2023).

Font, O., Moreno, T., Querol, X., Martins, V., Sánchez Rodas, D., Miguel, E. de, et al., 2019. Origin and speciation of major and trace PM elements in the Barcelona subway system. Transp. Res. Part D: Transp. Environ. 72 (1506–1516), 17–35. https://www.researchgate.net/publication/334141687_Origin_and_speciation_of_major_and_trace_PM_elements_in_the_Barcelona_subway_system.

Fortoul, T., Rodríguez-Lara, V., González-Villalva, A., Rojas-Lemus, M., Colín-Barenque, L., Bizarro-Nevares, P., et al., 2015. Health effects of metals in particulate matter. https://www.semanticscholar.org/paper/Health-Effects-of-Metals-in-Particulate-Matter-Fortoul-Rodr%C3%ADguez-Lara/9e1dcb26db219f654d2ab5e1a1c301fe25a25661.

Ghio, A.J., Dailey, L.A., Richards, J.H., Jang, M., 2009. Acid and organic aerosol coatings on magnetic nanoparticles increase iron concentrations in human airway epithelial cells. Inhal. Toxicol. 21 (8), 659–667. https://doi.org/10.1080/08958370802406282.

Ghio, A.J., Smith, C.B., Madden, M.C., 2012. Diesel exhaust particles and airway inflammation. Curr. Opin. Pulm. Med. 18 (2), 144–150. https://journals.lww.com/co-pulmonarymedicine/fulltext/2012/03000/Diesel_exhaust_particles_and_airway_inflammation.10.aspx.

Grigoratos, T., Martini, G., 2014. Non-exhaust traffic related emissions – Brake and tyre wear PM. 1831-9424. https://publications.jrc.ec.europa.eu/repository/handle/JRC89231.

Grigoratos, T., Martini, G., 2015. Brake wear particle emissions: a review. Environ. Sci. Pollut. Res. 22 (4), 2491–2504. https://pubmed.ncbi.nlm.nih.gov/25318420/.

Hagino, H., Oyama, M., Sasaki, S., 2016. Laboratory testing of airborne brake wear particle emissions using a dynamometer system under urban city driving cycles. Atmos. Environ. 131, 269–278. https://www.sciencedirect.com/science/article/pii/S135223101630125X.

Heim, M., Mullins, B.J., Umhauer, H., Kasper, G., 2008. Performance evaluation of three optical particle counters with an efficient "multimodal" calibration method. J. Aerosol Sci. 39 (12), 1019–1031. https://doi.org/10.1016/j.jaerosci.2008.07.006.

Hejazy, M., Koohi, M.K., Pour, Bassiri Mohamad, A., Najafi, D., 2018. Toxicity of manufactured copper nanoparticles - a review. Nanomed. Res. J. 3 (1), 1–9. http://www.nanomedicine-rj.com/article_31894.html.

Hinds, W.C., Zhu, Y., 2022. Aerosol Technology: Properties, Behavior, and Measurement of Airborne Particles. Wiley, Hoboken, NJ.

Hopkins, L.E., Laing, E.A., Peake, J.L., Uyeminami, D., Mack, S.M., Li, X., et al., 2018. Repeated iron–soot exposure and nose-to-brain transport of inhaled ultrafine particles. Toxicol. Pathol. 46 (1), 75–84. https://www.ncbi.nlm.nih.gov/pmc/articles/PMC6405220/.

Iijima, A., Sato, K., Yano, K., Tago, H., Kato, M., Kimura, H., et al., 2007. Particle size and composition distribution analysis of automotive brake abrasion dusts for the evaluation of antimony sources of airborne particulate matter. Atmos. Environ. 41 (23), 4908–4919. https://www.sciencedirect.com/science/article/pii/S1352231007001409.

Jung, H.-J., Kim, B., Ryu, J., Maskey, S., Kim, J.-C., Sohn, J., et al., 2010. Source identification of particulate matter collected at underground subway stations in Seoul, Korea using quantitative single-particle analysis. Atmos. Environ. 44 (19), 2287–2293. https://www.sciencedirect.com/science/article/pii/S1352231010002852.

Jung, M.H., Kim, H.R., Park, Y.J., Park, D.S., Chung, K.H., Oh, S.M., 2012. Genotoxic effects and oxidative stress induced by organic extracts of particulate matter (PM 10) collected from a subway tunnel in Seoul, Korea. Mutat. Res. 749 (1–2), 39–47. https://www.sciencedirect.com/science/article/pii/S1383571812002690.

Kanti Das, T., Wati, M.R., Fatima-Shad, K., 2014. Oxidative stress gated by Fenton and Haber Weiss reactions and its association with Alzheimer's disease. Arch. Neurosci. 2 (3) https://doi.org/10.5812/archneurosci.20078.

Karlsson, H.L., Ljungman, A.G., Lindbom, J., Möller, L., 2006. Comparison of genotoxic and inflammatory effects of particles generated by wood combustion, a road

simulator and collected from street and subway. Toxicol. Lett. 165 (3), 203–211. https://www.sciencedirect.com/science/article/pii/S0378427406001238.
Karlsson, H.L., Holgersson, A., Möller, L., 2008. Mechanisms related to the genotoxicity of particles in the subway and from other sources. Chem. Res. Toxicol. 21 (3), 726–731. https://doi.org/10.1021/tx7003568.
Kim, K.-H., Ho, D.X., Jeon, J.-S., Kim, J.-C., 2012. A noticeable shift in particulate matter levels after platform screen door installation in a Korean subway station. Atmos. Environ. 49, 219–223. https://www.sciencedirect.com/science/article/pii/S1352231011012453.
Knight, L.J., Parker-Jurd, F.N.F., Al-Sid-Cheikh, M., Thompson, R.C., 2020. Tyre wear particles: an abundant yet widely unreported microplastic? Environ. Sci. Pollut. Res. 27 (15), 18345–18354. https://doi.org/10.1007/s11356-020-08187-4.
Kumar, P., Zavala-Reyes, J.C., Kalaiarasan, G., Abubakar-Waziri, H., Young, G., Mudway, I., et al., 2023. Characteristics of fine and ultrafine aerosols in the London underground. Sci. Total Environ. 858 (Pt 1), 159315. https://www.sciencedirect.com/science/article/pii/S0048969722064142.
Laborda, F., Bolea, E., Jiménez-Lamana, J., 2014. Single particle inductively coupled plasma mass spectrometry: a powerful tool for nanoanalysis. Anal. Chem. 86 (5), 2270–2278. https://doi.org/10.1021/ac402980q.
Lay, J.C., Bennett, W.D., Ghio, A.J., Bromberg, P.A., Costa, D.L., Kim, C.S., et al., 1999. Cellular and biochemical response of the human lung after intrapulmonary instillation of ferric oxide particles. Am. J. Respir. Cell Mol. Biol. 20 (4), 631–642. https://doi.org/10.1165/ajrcmb.20.4.3355.
Longo, A.F., Feng, Y., Lai, B., Landing, W.M., Shelley, R.U., Nenes, A., et al., 2016. Influence of atmospheric processes on the solubility and composition of iron in Saharan dust. Environ. Sci. Technol. 50 (13), 6912–6920. https://doi.org/10.1021/acs.est.6b02605.
Loxham, M., Nieuwenhuijsen, M.J., 2019. Health effects of particulate matter air pollution in underground railway systems - a critical review of the evidence. Part. Fibre Toxicol. 16 (1), 12. https://doi.org/10.1186/s12989-019-0296-2.
Morawska, L., Buonanno, G., 2021. The physics of particle formation and deposition during breathing. Nat. Rev. Phys. 3 (5), 300–301. https://www.nature.com/articles/s42254-021-00307-4.
Moreno, T., Martins, V., Querol, X., Jones, T., BéruBé, K., Minguillón, M.C., et al., 2015. A new look at inhalable metalliferous airborne particles on rail subway platforms. Sci. Total Environ. 505, 367–375. https://pubmed.ncbi.nlm.nih.gov/25461038/.
Morgan, J., Bell, R., Jones, A.L., 2020. Endogenous doesn't always mean innocuous: a scoping review of iron toxicity by inhalation. J. Toxicol. Environ. Health B Crit. Rev. 23 (3), 107–136. https://doi.org/10.1080/10937404.2020.1731896.
mvg.de, R., 2023. Entlastungsspange U9 | Münchner Verkehrsgesellschaft mbH. https://www.mvg.de/ueber/mvg-projekte/bauprojekte/u9.html (accessed 18 September 2023).
Niska, K., Santos-Martinez, M.J., Radomski, M.W., Inkielewicz-Stepniak, I., 2015. CuO nanoparticles induce apoptosis by impairing the antioxidant defense and detoxification systems in the mouse hippocampal HT22 cell line: protective effect of crocetin. Toxicology 29 (4), 663–671. https://www.sciencedirect.com/science/article/pii/S0887233315000211.
Sankhe, K., Khan, T., Bhavsar, C., Momin, M., Omri, A., 2019. Selective drug deposition in lungs through pulmonary drug delivery system for effective management of drug-resistant TB. Expert Opin. Drug Deliv. 16 (5), 525–538. https://doi.org/10.1080/17425247.2019.1609937.
Son, Y.-S., Salama, A., Jeong, H.-S., Kim, S., Jeong, J.-H., Lee, J., et al., 2013. The effect of platform screen doors on PM10 levels in a subway station and a trial to reduce PM10 in tunnels. ajae 7 (1), 38–47. https://doi.org/10.5572/ajae.2013.7.1.038.
Storch, L., Hamatscheck, C., Hesse, D., Feist, F., Bachmann, T., Eichler, P., et al., 2023. Comprehensive Analysis of Current Primary Measures to Mitigate Brake Wear Particle Emissions from Light-Duty Vehicles. 2073-4433 14(4), 712. https://publications.jrc.ec.europa.eu/repository/handle/JRC133217.
Stueckle, T.A., Davidson, D.C., Derk, R., Kornberg, T.G., Schwegler-Berry, D., Pirela, S.V., et al., 2017. Evaluation of tumorigenic potential of CeO2 and Fe2O3 engineered nanoparticles by a human cell in vitro screening model. NanoImpact 6, 39–54. https://www.sciencedirect.com/science/article/pii/S2452074816300994.
Sun, S., Zheng, N., Wang, S., Li, Y., Hou, S., An, Q., et al., 2022. Inhalation bioaccessibility and risk assessment of metals in PM2.5 based on a multiple-path particle dosimetry model in the Smelting District of Northeast China. Int. J. Environ. Res. Public Health 19 (15). https://www.ncbi.nlm.nih.gov/pmc/articles/PMC9331668/.
Thorley, A.J., Ruenraroengsak, P., Potter, T.E., Tetley, T.D., 2014. Critical determinants of uptake and translocation of nanoparticles by the human pulmonary alveolar epithelium. ACS Nano 8 (11), 11778–11789. https://pubmed.ncbi.nlm.nih.gov/25360809/.
Totlandsdal, A.I., Cassee, F.R., Schwarze, P., Refsnes, M., Låg, M., 2010. Diesel exhaust particles induce CYP1A1 and pro-inflammatory responses via differential pathways in human bronchial epithelial cells. Part. Fibre Toxicol. 7 (1), 41. https://doi.org/10.1186/1743-8977-7-41.
Trambahn.de, 2023. U-Bahn Fahrzeuge | trambahn. https://www.trambahn.de/u-bahn fahrzeuge (accessed 18 September 2023).
Trickler, W.J., Lantz-McPeak, S.M., Robinson, B.L., Paule, M.G., Slikker, W., Biris, A.S., et al., 2014. Porcine brain microvessel endothelial cells show pro-inflammatory response to the size and composition of metallic nanoparticles. Drug Metab. Rev. 46 (2), 224–231. https://doi.org/10.3109/03602532.2013.873450.
U-Bahn München, 2023a. Stromversorgung. https://www.u-bahn-muenchen.de/betrieb/stromversorgung/ (accessed 19 September 2023a).
U-Bahn München, 2023b. U-Bahnhof Hauptbahnhof (U4, U5). https://www.u-bahn-muenchen.de/netz/bahnhoefe/ho/ (accessed 04 November 2023b).
Walther, E., Bogdan, M., 2017. A novel approach for the modelling of air quality dynamics in underground railway stations. Transp. Res. Part D: Transp. Environ. 56, 33–42. https://www.sciencedirect.com/science/article/pii/S1361920917301487.
Wang, B.-Q., Liu, J.-F., Ren, Z.-H., Chen, R.-H., 2016. Concentrations, properties, and health risk of PM2.5 in the Tianjin City subway system. Environ. Sci. Pollut. Res. 23 (22), 22647–22657. https://doi.org/10.1007/s11356-016-7444-0.
Yang, C., Cai, G., Li, X., Bo, J., 2016. Study on third rail current collector shoes wear of metro trains. In: International Conference on Logistics, Informatics and Service Sciences (LISS), pp. 1–4. https://doi.org/10.1109/LISS.2016.7854552.
Zhang, Y., Schauer, J.J., Shafer, M.M., Hannigan, M.P., Dutton, S.J., 2008. Source apportionment of in vitro reactive oxygen species bioassay activity from atmospheric particulate matter. Environ. Sci. Technol. 42 (19), 7502–7509. https://doi.org/10.1021/es800126y.
Zhang, M., Shao, L., Jones, T., Feng, X., Ge, S., Yang, C.-X., et al., 2022. Atmospheric iron particles in PM2.5 from a subway station, Beijing, China. Atmos. Environ. 283, 119175. https://www.sciencedirect.com/science/article/pii/S1352231022002400.
Zhou, H., Duan, F., Liu, Z., Chen, L., Song, Y., Zhang, Y., 2022. Study on electric spark discharge between pantograph and catenary in electrified railway. IET Electr. Syst. Trans. 12 (2), 128–142. https://doi.org/10.1049/els2.12043.